

LETTER TO THE EDITOR

Detection of a large-scale organized 2 kG order magnetic field in the Herbig Ae star HD 179218

S. P. Järvinen¹, S. Hubrig¹, M. Schöller², I. Ilyin¹, H. N. Adigozalzade³, N. Z. Ismailov³, U. Z. Bashirova³, and S. A. Alishov³

¹ Leibniz-Institut für Astrophysik Potsdam (AIP), An der Sternwarte 16, 14482 Potsdam, Germany
e-mail: sjarvinen@aip.de

² European Southern Observatory, Karl-Schwarzschild-Str. 2, 85748 Garching, Germany

³ N. Tusi Shamakhy Astrophysical Observatory, settl. Y. Mammadaliyev, 5626 Shamakhy, Azerbaijan

Received 30 April 2026 / Accepted 18 May 2026

ABSTRACT

Context. While about two dozen Herbig Ae/Be stars have been reported to be magnetic, only two of them, HD 101412 and HD 190073, have had their magnetic field geometries studied in the past. The knowledge of the magnetic field structure is important to understanding how magnetospheric accretion works in these stars.

Aims. We aim to study in detail the spectral and magnetic variability of HD 179218, which is necessary to put constraints on its magnetic field geometry.

Methods. We measured the mean longitudinal magnetic field, $\langle B_z \rangle$, from newly acquired and archival high-resolution spectropolarimetric observations of HD 179218 using the least-squares deconvolution technique. Additionally, we studied the spectral variability of the hydrogen lines using dynamical spectra.

Results. Based on our analysis of the Stokes V spectra of HD 179218, we report for the first time the definite detection of a magnetic field. Using a slightly refined rotation period of $P_{\text{rot}} = 1.34102$ d, we constrained its geometry as follows: an estimated magnetic obliquity angle of $\beta = 79.9 \pm 0.7^\circ$ and a dipole strength of $B_d = 2142 \pm 52$ G. The $\langle B_z \rangle$ variation is best fitted by the superposition of a sine wave and of its first harmonic, but more spectropolarimetric observations are necessary to test the impact of the limited measurement precision and the uneven coverage of the rotation cycle. The strongest emission in the $H\alpha$ and $H\beta$ line profiles in the medium-resolution spectra acquired in 2025 was detected close to the phases of the best visibility of the magnetic poles. HD 179218 is the second Herbig Ae/Be star after HD 190073 for which a first snapshot of a magnetosphere is presented.

Key words. stars: magnetic field – stars: individual: HD 179218 – stars: pre-main sequence – stars: variables: T Tauri, Herbig Ae/Be – techniques: polarimetric

1. Introduction

Observations of the disk properties of intermediate mass Herbig Ae/Be stars suggest a close parallel to T Tauri stars. Herbig Ae/Be stars and classical T Tauri stars are surrounded by active accretion disks, and (probably) most of the excess emission seen at various wavelength regions can be attributed to the interaction of the disk with a magnetically active star (e.g. Muzerolle et al. 2004). This interaction is generally referred to as magnetospheric accretion (MA). However, T Tauri stars generally have kilogauss-order complex magnetic field structures, while Herbig Ae/Be stars have been reported to possess much simpler and far weaker fields, frequently below 100 G (e.g. Hubrig et al. 2009, 2011, 2015). While about two dozen Herbig Ae/Be stars are reported to be magnetic, only two Herbig Ae/Be stars, HD 101412 and HD 190073, have had their magnetic field geometries constrained. These two stars have rather long rotation periods (P_{rot}), with 42.076 ± 0.017 d for HD 101412 and 51.70 ± 0.06 d for HD 190073. It has been shown that these Herbig Ae/Be stars exhibit single-wave variations of the longitudinal magnetic field during the stellar rotation cycle. This behaviour is usually considered as evidence of a dominant dipolar contribution to the magnetic field topology. Among the studied stars, the Herbig Ae star HD 101412 possesses the strongest magnetic field, with

the measured mean magnetic field modulus varying from 2.5 to 3.5 kG (e.g. Hubrig et al. 2010).

To understand how MA works in Herbig Ae/Be stars, knowledge of the magnetic field structure is indispensable. However, most Herbig Ae/Be stars are faint and require a considerable amount of telescope time. Therefore, the multi-epoch spectrophotometric observations necessary to estimate their rotation period and the magnetic field strength distribution over the rotation period are rare. The most recent study of the Herbig Ae star HD 190073 with a nearly face-on disk orientation carried out by Järvinen et al. (2025) demonstrated that even stars with rather weak longitudinal magnetic fields of the order of a few tens of gauss possess sizeable magnetospheres. The authors reported that for HD 190073, with a maximum longitudinal magnetic field of only 34 G, 2D magnetohydrodynamical simulations show the presence of a compact magnetosphere with a radius of about $3 R_*$ and a wind flow extending over tens of stellar radii (R_*). Järvinen et al. (2025) used archival observations of HD 190073 acquired by different spectropolarimeters from 2012 to 2019 and were able not only to determine the rotation and magnetic period but also, for the first time, investigate in detail the remarkable variability of the emission Balmer line profiles of $H\alpha$, $H\beta$, and $H\gamma$ over the rotation period. The dynamical spec-

tra constructed for the hydrogen line profiles revealed a ring-like magnetospheric structure appearing at the rotation phase of best visibility of the positive magnetic pole.

In this study we present our new spectropolarimetric observations of the Herbig Ae star HD 179218. The star was extensively studied by [Ismailov et al. \(2024\)](#), who reported the rotation period $P_{\text{rot}} = 1.341 \pm 0.002$ d when using spectra obtained between 2015 with a resolution $R = 14\,000$ and 2021 ($R = 28\,000$) to study the variability of the $H\beta$ and the $\text{He I } 5876$ lines. [Cody et al. \(2025\)](#) found no periodicity in the Transiting Exoplanet Survey Satellite ([Ricker et al. 2016](#)) observations. According to [Fedele et al. \(2008\)](#), HD 179218 has two rings of dust at 1 and 20 au and a compact gas emitting region between 1 and 6 au. [Mendigutía et al. \(2017\)](#) reported that MA is able to reproduce the bulk of the $H\alpha$ emission shown by HD 179218, confirming previous estimates from MA shock modeling with a mass accretion rate of $10^{-8} M_{\odot} \text{ yr}^{-1}$ and an inclination to the line of sight between 30° and 50° . Most recent interferometric observations with GRAVITY indicate a disk inclination to the line of sight of $i = 54^{+8}_{-10}$ ([GRAVITY Collaboration et al. 2024](#)).

The first attempt to measure the magnetic field of HD 179218 was carried out by [Hubrig et al. \(2009\)](#), based on low-resolution FOCal Reducer low dispersion Spectrograph (FORIS; [Appenzeller et al. 1998](#)) observations on a single epoch. However, the measurement accuracy was too low to be able to announce the detection of a magnetic field. A further attempt was made by [Alecian et al. \(2013\)](#), this time using the high-resolution Echelle Spectropolarimetric Device for the Observation of Stars (ESPaDONs; [Donati et al. 2006](#)) and Narval ([Aurière 2003](#)) spectropolarimeters on four observing epochs. Again, no definite detection was reported. These observations are publicly available from the Canada-France-Hawaii Telescope (CFHT) and Polar-Base ([Petit et al. 2014](#)) data archives.

To clarify the magnetic nature of HD 179218, we obtained seven additional high-resolution spectropolarimetric observations in 2022 and 2025 with the High Accuracy Radial velocity Planet Searcher polarimeter (HARPSpol; [Snik et al. 2008](#)) attached to the 3.6 m European Southern Observatory (ESO) telescope at the La Silla Observatory in Chile. In Sect. 2 we describe the observational material used in this work, and we present the results of our magnetic field measurements using our own and archival data, the obtained constraints on the magnetic field geometry, and the appearance of dynamical spectra constructed for the $H\alpha$, $H\beta$, and $\text{He I } 5876$ lines. In the Sect. 3 we discuss our new results in the light of the current knowledge of magnetism among Herbig Ae/Be stars and new possible directions in their studies.

2. Observations and magnetic field measurements

The spectropolarimetric observations analysed in this paper were obtained on April 24 and 30, 2022, as well as on July 5 to 9, 2025, with HARPSpol. The target was also observed in spectropolarimetric mode with ESPaDONs, installed at the CFHT, during February 21 and August 26, 2005, and with Narval installed at the Bernard Lyot Telescope at the Pic du Midi, France, during September 15, 2007, and October 3, 2009. However, the exposure time for the first Narval observation was only 600 s, making these data unusable for our analysis. HARPSpol provides a resolving power of about 115 000, whereas for ESPaDONs and Narval the spectral resolution is about 65 000. A summary of all observations is presented in Table 1.

HD 179218 has also been intensively observed at medium resolution with the 2 m telescope of the Shamakhy Astrophys-

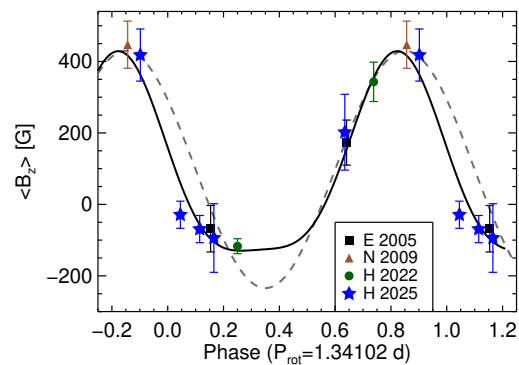


Fig. 1. Magnetic phase curve for HD 179218. The measured $\langle B_z \rangle$ values presented in Table 1 have been phased with the refined period $P_{\text{rot}} = 1.34102$ d. Different symbols with different colours refer to observations acquired with ESPaDONs in 2005, Narval in 2009, and HARPSpol in 2022 and 2025. The dashed line is the sinusoidal fit to the data points, assuming a purely dipolar field configuration, whereas the solid line includes a contribution of the first harmonic.

ical Observatory. We used the two most complete datasets to monitor the variability of the $H\alpha$, $H\beta$, and $\text{He I } 5876$ lines with dynamical spectra. The first data set consists of 28 individual spectra obtained between May and August 2015 with a resolution $R = 14\,000$. The details of the observations and the setup are given in [Ismailov et al. \(2019\)](#). The second dataset used in our study was obtained between June and August 2025, with a total of 45 spectra at $R = 28\,000$. The details of these observations are presented in Table A.1 in the Appendix.

The mean longitudinal magnetic field $\langle B_z \rangle$, accessible through high-resolution spectropolarimetric observations, is the line-of-sight component of the magnetic field weighted with the line intensity and averaged over the visible hemisphere. It is strongly dependent on the viewing angle between the field orientation and the observer and is modulated as the star rotates. As in our previous studies (e.g. [Järvinen et al. 2025](#); [Hubrig et al. 2025](#)), we employed the least-squares deconvolution (LSD) technique following the description given by [Donati et al. \(1997\)](#). This technique allows the accuracy of the mean longitudinal magnetic field determination to be increased. The parameters for the individual lines are based on information provided by the Vienna Atomic Line Database (VALD3; [Kupka et al. 2011](#)) using an effective temperature $T_{\text{eff}} = 9500 \pm 250$ K and a surface gravity $\log g = 3.95 \pm 0.10$ ([Wichittanakom et al. 2020](#)) and a detection threshold of 0.1. To evaluate the detected features, we followed the false alarm probability (FAP) based on reduced χ^2 test statistics ([Donati et al. 1992](#)): The presence of the Zeeman feature is considered a definite detection (DD) if $\text{FAP} \leq 10^{-5}$, a marginal detection (MD) if $10^{-5} < \text{FAP} \leq 10^{-3}$, and a non-detection (ND) if $\text{FAP} > 10^{-3}$.

The results of our magnetic field measurements and the corresponding FAP values are given in Table 1, while the obtained LSD profiles ordered by increasing rotation phases are shown in Appendix B in Fig. B.1. Since the data used were obtained over 20 years and the rotation period of 1.341 d is very short and not especially accurate, the measured $\langle B_z \rangle$ strengths plotted against the phase displayed noticeable dispersion with phase shifts between similar field strength values. After the refinement of the period and taking into account the phase shift between the field strength measured on August 26, 2005, and the measurements on July 7, 2025, we obtained a period of 1.34102 d. In Fig. 1 we display the $\langle B_z \rangle$ plotted against the rotation phase and fitted by a sine curve (the dashed line), under the assumption that

Table 1. Logbook of the high-resolution spectropolarimetric observations and the results of the magnetic field measurements.

Inst	MJD	φ	S/N	Line mask	FAP	Det. flag	$\langle B_z \rangle$ [G]
E	53422.649074	0.153	177	MgSiTiCrFe	9×10^{-4}	MD	-68 ± 65
E	53608.363169	0.641	396	CrFe	5×10^{-7}	DD	173 ± 63
N	55107.912442	0.856	413	MgSiTiCrFe	1×10^{-4}	MD	447 ± 66
H	59693.387609	0.250	261	SiCrFe	2×10^{-7}	DD	-117 ± 21
H	59699.406061	0.738	220	MgSiFe	9×10^{-7}	DD	343 ± 55
H	60861.141508	0.045	279	SiCaTiCrFe	8×10^{-8}	DD	-29 ± 38
H	60861.302527	0.165	216	TiCrFe	2×10^{-5}	MD	-94 ± 96
H	60862.290035	0.902	191	SiTiCrFe	1×10^{-7}	DD	418 ± 73
H	60863.272849	0.635	242	TiCrFe	2×10^{-4}	MD	202 ± 106
H	60865.257535	0.115	290	CaSiTiCrFe	3×10^{-5}	MD	-69 ± 38

Notes. The first column shows the instrument used: ‘E’ indicates ESPaDOnS, ‘N’ Narval, and ‘H’ HARPSpol. This is followed by the modified Julian date (MJD) values at the middle of the exposure, the corresponding phase (MJD for phase zero $T_0 = 59\,693.052435$, $P_{\text{rot}} = 1.34102$ d), and the signal-to-noise ratio measured in the Stokes I spectra in the spectral region around 5000 \AA . The line mask used, the FAP values, the detection flag (with ‘DD’ meaning ‘definite detection’ and ‘MD’ standing for ‘marginal detection’), and the measured LSD mean longitudinal magnetic field strength are presented in Columns 5–8.

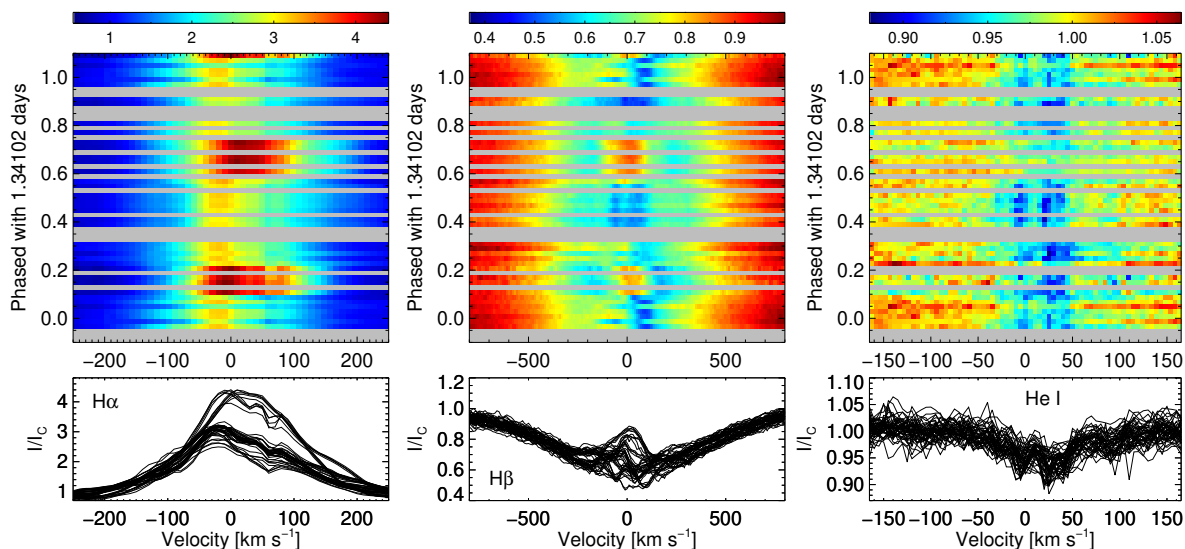


Fig. 2. Dynamical spectra constructed for the $H\alpha$ (left), $H\beta$ (middle), and $He\ I\ 5876$ (right) line profiles. They are based on medium resolution spectra obtained in 2025 and are phased with $P_{\text{rot}} = 1.34102$ d. The overplotted individual line profiles are shown in the bottom panels.

the field geometry is a pure dipole. Reasonable evidence that the field geometry is predominantly dipolar follows from the appearance of the dynamical spectra constructed for the $H\alpha$ and $H\beta$ line profiles observed using the medium-resolution dataset from 2025. As presented in Fig. 2, the hydrogen line profiles show a clear increase of emission twice over the rotation cycle. As recently discussed by Järvinen et al. (2025) and Hubrig et al. (2025), such an increase is related to a stellar magnetosphere and generally occurs when one of the magnetic poles comes into sight as the star rotates. Also, other spectral lines exhibit a distinct variability. In Fig. 2 we show that despite the $He\ I\ 5876$ line profiles being rather weak and noisy, they generally follow the behaviour of the $H\beta$ profiles. At some phases both lines display a double-absorption structure in the line cores, best visible around the phase 0.5. It is not clear whether these absorptions are related to the surrounding hot inner disk region mentioned by Kokoulina et al. (2021). In addition, in Fig. C.1 in the Appendix we show the combined variability of Ti, Cr, and Fe lines. In contrast to the observations acquired in 2025, the emission

strengths in the $H\alpha$ and $H\beta$ lines observed in 2015 and displayed in Fig. D.1 are much lower and have no clear periodical changes in their line profiles. An annual change in the hydrogen line profiles was previously observed in HD 190073 by Järvinen et al. (2025). The authors speculated that this was due to an interaction with a secondary body in the system causing an increase in the wind outflow and producing a partial screening of the magnetosphere.

Using the strongest measured $\langle B_z \rangle$ of 447 ± 66 G and employing the relation $B_d \geq 3|\langle B_z \rangle|$ (Babcock 1958), we estimate the minimum dipole strength, B_d , to be about 1.34 kG. Assuming a rotation period P_{rot} of 1.34102 d and a stellar radius R_* of $3.59 \pm 0.10 R_\odot$ (Guzmán-Díaz et al. 2021), we obtained an equatorial velocity of $v_{\text{eq}} = 135.46 \pm 3.77 \text{ km s}^{-1}$. Using $v \sin i = 68.8 \pm 2.9 \text{ km s}^{-1}$ from the study of Alecian et al. (2013), the angle between the rotation axis and the line of sight i is $30.5 \pm 1.7^\circ$. The general description for the strength of the observed longitudinal magnetic field for a simple centred dipole was presented by Preston (1967). The relative amplitude

of variation of the fitted longitudinal magnetic field phase curve is usually characterised by the parameter r , representing the ratio between $\langle B_z \rangle_{\min}$ and $\langle B_z \rangle_{\max}$. Here, assuming a dipolar field, with $\langle B_z \rangle_{\max} = 430 \pm 4$ G and $\langle B_z \rangle_{\min} = -234 \pm 4$ G, we have $r = -0.54 \pm 0.10$. Using

$$r = \frac{\langle B_z \rangle_{\min}}{\langle B_z \rangle_{\max}} = \frac{\cos \beta \cos i - \sin \beta \sin i}{\cos \beta \cos i + \sin \beta \sin i}, \quad (1)$$

we calculated an obliquity angle of $\beta = 79.9 \pm 0.7^\circ$. With a limb-darkening coefficient of 0.5 (Claret 2019), we obtained a polar magnetic field strength of $B_d = 2142 \pm 52$ G.

As demonstrated in Fig. 1, the $\langle B_z \rangle$ phase curve shows a degree of anharmonicity that requires a contribution of a first harmonic. The solid line in this plot represents a fit of the observations by a superposition of a dipole and a quadrupole field at the centre of the star. Clearly, more measurements of $\langle B_z \rangle$ are necessary to be able to decide whether it is possible that the anharmonic variation curve actually results from some combination of the limited precision of the measurements and their uneven coverage over the rotation cycle.

3. Discussion

HD 179218 is the third Herbig Ae/Be star with a known rotation period, and it hosts the second strongest magnetic field (after that of HD 101412), with a 2 kG order dipolar component. A rotation period of 1.341 d was estimated from the variable position of the red boundary of the absorption component of the inverse P Cyg-type profile of H β by Ismailov et al. (2024), who assumed that this variability is caused by MA. A similar procedure using structural kinematic features of the gas environment was previously successfully applied using near-infrared observations of the strongly magnetic Herbig Ae star HD 101412 (Schöller et al. 2016). It would be worthwhile to apply such a procedure to other Herbig Ae/Be stars to estimate their rotation periods. However, since Herbig Ae/Be stars are complex systems with surrounding protoplanetary disks and diverse interactions between star, gas, and dust, extensive time series over hours, days, and months are necessary to disentangle the contributions from the different system components.

It is notable that based on the variability of the Balmer line profiles and the colour indices in the $U BV RI$ system monitored over several years, Ismailov et al. (2025) also suggested the presence of longer periods from 37.5 to 737 d, which may be explained by the presence of a distant companion and, possibly, one or more distant exoplanets around HD 179218. The dynamical spectra of the H α and H β line profiles phased with the period of 37.5 d are presented in Fig. D.2 in the Appendix. Even if the phase coverage is poor, some hints of a structure with maximum emission in phases between 0.15 and 0.4 can be observed. Also the absence of periodicity over the 1.341 d rotation period in the Balmer line profiles in the spectra acquired in 2015 suggests that some kind of dynamical process (probably due to the presence of a companion) takes place around the central star. According to Thomas et al. (2023), who used adaptive optics infrared imaging surveys, one of the possible companions, HD 179218 B, is located at about 2.5". That is too far to have an important dynamical impact, and no close companion was detected using interferometric observations. MATISSE L-band observations of HD 179218 by Kokoulina et al. (2021) reported on the presence of two separate dust populations: a region filled with stochastically heated, very small (nano-)carbon grains within 10 au and a colder outer disk for which the infrared emission is dominated by larger, probably micrometre-sized, grains.

The presented magnetic phase curve of HD 179218 based on the longitudinal magnetic field measurements carried out on ten observing epochs indicates a more complex magnetic topology than a pure dipole and suggests a contribution of a quadrupolar field component. It is not clear whether this more complex field structure, if confirmed by future observations, is due to the faster rotation of this star in comparison to the rather slow rotation of the two previously studied Herbig Ae/Be stars (HD 101412 and HD 190073) with dipole fields. Obviously, additional spectropolarimetric observations of HD 179218 with a dense coverage of the rotation cycle will be valuable to ascertaining the structure of its magnetic field in more detail.

Acknowledgements. We thank the referee, P. Petit, for his comments. This work is based on observations made with ESO telescopes at the La Silla Paranal Observatory under programme IDs 0109.C-0265(A) and 0115.D-2108(A) publicly available from the ESO Archive, on observations collected at the Canada-France-Hawaii Telescope (CFHT), which is operated by the National Research Council of Canada, the Institut National des Sciences de l'Univers of the Centre National de la Recherche Scientifique of France, and the University of Hawaii, and on observations collected at the Bernard Lyot Telescope at the Pic du Midi de Bigorre, France, which is managed by the Observatoire Midi Pyrénées.

References

- Alecian, E., Wade, G. A., Catala, C., et al. 2013, MNRAS, 429, 1001
 Appenzeller, I., Fricke, K., Fürstig, W., et al. 1998, The Messenger, 94, 1
 Aurière, M. 2003, in EAS Publications Series, Vol. 9, EAS Publications Series, ed. J. Arnaud & N. Meunier (EDP), 105
 Babcock, H. W. 1958, ApJS, 3, 141
 Claret, A. 2019, Research Notes of the American Astronomical Society, 3, 17
 Cody, A. M., Hillenbrand, L. A., Chandragiri, S., & Morgan, M. 2025, ApJ, 994, 253
 Donati, J.-F., Catala, C., Landstreet, J. D., & Petit, P. 2006, in Astronomical Society of the Pacific Conference Series, Vol. 358, Solar Polarization 4, ed. R. Casini & B. W. Lites, 362
 Donati, J.-F., Semel, M., Carter, B. D., Rees, D. E., & Collier Cameron, A. 1997, MNRAS, 291, 658
 Donati, J.-F., Semel, M., & Rees, D. E. 1992, A&A, 265, 669
 Fedele, D., van den Ancker, M. E., Acke, B., et al. 2008, A&A, 491, 809
 GRAVITY Collaboration, Garcia Lopez, R., Natta, A., et al. 2024, A&A, 684, A43
 Guzmán-Díaz, J., Mendigutía, I., Montesinos, B., et al. 2021, A&A, 650, A182
 Hubrig, S., Carroll, T. A., Scholler, M., & Ilyin, I. 2015, MNRAS, 449, L118
 Hubrig, S., Järvinen, S. P., Ilyin, I., & Schöller, M. 2025, A&A, 696, L15
 Hubrig, S., Mikulášek, Z., González, J. F., et al. 2011, A&A, 525, L4
 Hubrig, S., Schöller, M., Savanov, I., et al. 2010, Astronomische Nachrichten, 331, 361
 Hubrig, S., Stelzer, B., Schöller, M., et al. 2009, A&A, 502, 283
 Ismailov, N. Z., Bashirova, U. Z., & Adigezalzade, A. N. 2019, Astrophysical Bulletin, 74, 300
 Ismailov, N. Z., Pogodin, M. A., Kholtygin, A. F., Adigozalzade, H. N., & Bashirova, U. Z. 2024, Astrophysical Bulletin, 79, 464
 Ismailov, N. Z., Pogodin, M. A., Kholtygin, A. F., et al. 2025, Astrophysical Bulletin, 80, 14
 Järvinen, S. P., Hubrig, S., Küker, M., et al. 2025, A&A, 696, A155
 Kokoulina, E., Matter, A., Lopez, B., et al. 2021, A&A, 652, A61
 Kupka, F., Dubernet, M.-L., & VAMDC Collaboration. 2011, Baltic Astronomy, 20, 503
 Mendigutía, I., Oudmajer, R. D., Mourard, D., & Muzerolle, J. 2017, MNRAS, 464, 1984
 Mikailov, K. M., Musaev, F. A., Alekberov, I. A., Rustamov, B. N., & Khalilov, O. V. 2020, Kinematics and Physics of Celestial Bodies, 36, 22
 Muzerolle, J., D'Alessio, P., Calvet, N., & Hartmann, L. 2004, ApJ, 617, 406
 Petit, P., Louge, T., Théado, S., et al. 2014, PASP, 126, 469
 Preston, G. W. 1967, ApJ, 150, 547
 Ricker, G. R., Vanderspek, R., Winn, J., et al. 2016, in Society of Photo-Optical Instrumentation Engineers (SPIE) Conference Series, Vol. 9904, Space Telescopes and Instrumentation 2016: Optical, Infrared, and Millimeter Wave, ed. H. A. MacEwen, G. G. Fazio, M. Lystrup, N. Batalha, N. Siegler, & E. C. Tong, 99042B
 Schöller, M., Pogodin, M. A., Cahuasquí, J. A., et al. 2016, A&A, 592, A50
 Snik, F., Jeffers, S., Keller, C., et al. 2008, in Society of Photo-Optical Instrumentation Engineers (SPIE) Conference Series, Vol. 7014, Ground-based and Airborne Instrumentation for Astronomy II, ed. I. S. McLean & M. M. Casali, 701400
 Thomas, S. J., Rodgers, B., van der Blik, N. S., et al. 2023, AJ, 165, 135
 Wichittanakom, C., Oudmajer, R. D., Fairlamb, J. R., et al. 2020, MNRAS, 493, 234

Appendix A: Medium resolution observations

The details of the medium resolution observations collected during 2025 are presented in Table A.1. The observations were obtained with the ShAO fiber echelle spectrograph (ShaFES). The spectrograph is described in Mikailov et al. (2020) and the reduction in Ismailov et al. (2024).

Table A.1. Logbook of the 2025 medium resolution observations.

Date	UT	JD 2 460 000+	Exp [s]	S/N
11.06.2025	18:03	838.2521	3600	76
	19:19	838.3048	3600	74
14.06.2025	20:35	841.3576	3600	68
	21:25	842.3929	3600	66
19.06.2025	19:32	846.3138	3600	76
	20:32	846.3555	3600	76
	21:33	846.3979	3600	75
	22:33	846.4395	3600	79
25.06.2025	19:29	852.3118	3600	65
	20:30	852.3541	3600	63
	21:31	852.3965	3600	62
	22:32	852.4388	3600	63
26.06.2025	19:23	853.2976	3600	62
	20:23	853.3493	3600	69
	21:24	853.3916	3600	66
	22:25	853.4340	3600	63
27.06.2025	19:27	854.3104	3600	69
	20:23	854.3493	3600	60
	21:23	854.3909	3600	69
	22:28	854.4361	3600	65
28.06.2025	19:07	855.2965	3600	65
	20:07	855.3382	3600	63
	21:08	855.3805	3600	68
	22:09	855.4229	3600	66
11.07.2025	18:30	868.2708	3600	84
	19:33	868.3145	3000	81
	20:23	868.3493	3000	83
	21:13	868.3840	3000	82
	22:04	868.4194	3000	80
	22:54	868.4541	3000	81
12.07.2025	23:44	868.4889	3000	83
	21:55	869.4131	3000	79
	22:45	869.4479	3000	78
17.07.2025	19:28	874.3111	3000	76
	20:18	874.3458	3600	76
28.07.2025	19:51	885.3271	3600	61
01.08.2025	20:49	889.3674	3600	60
	21:50	889.4097	3600	59
	22:50	889.4514	3600	61
	23:50	889.4930	3600	62
30.08.2025	16:40	918.1944	3600	65
	17:41	918.2368	3600	64
	18:41	918.2784	3600	60
	19:41	918.3201	3600	66
	20:42	918.3625	3600	63

Notes. The first two columns give the date and universal time of the observations followed by the corresponding Julian date. The fourth column shows the exposure time and the fifth column gives the signal-to-noise ratio of the spectra.

Appendix B: LSD profiles

In Fig. B.1 we show the individual LSD profiles sorted according to the phase given in Table 1.

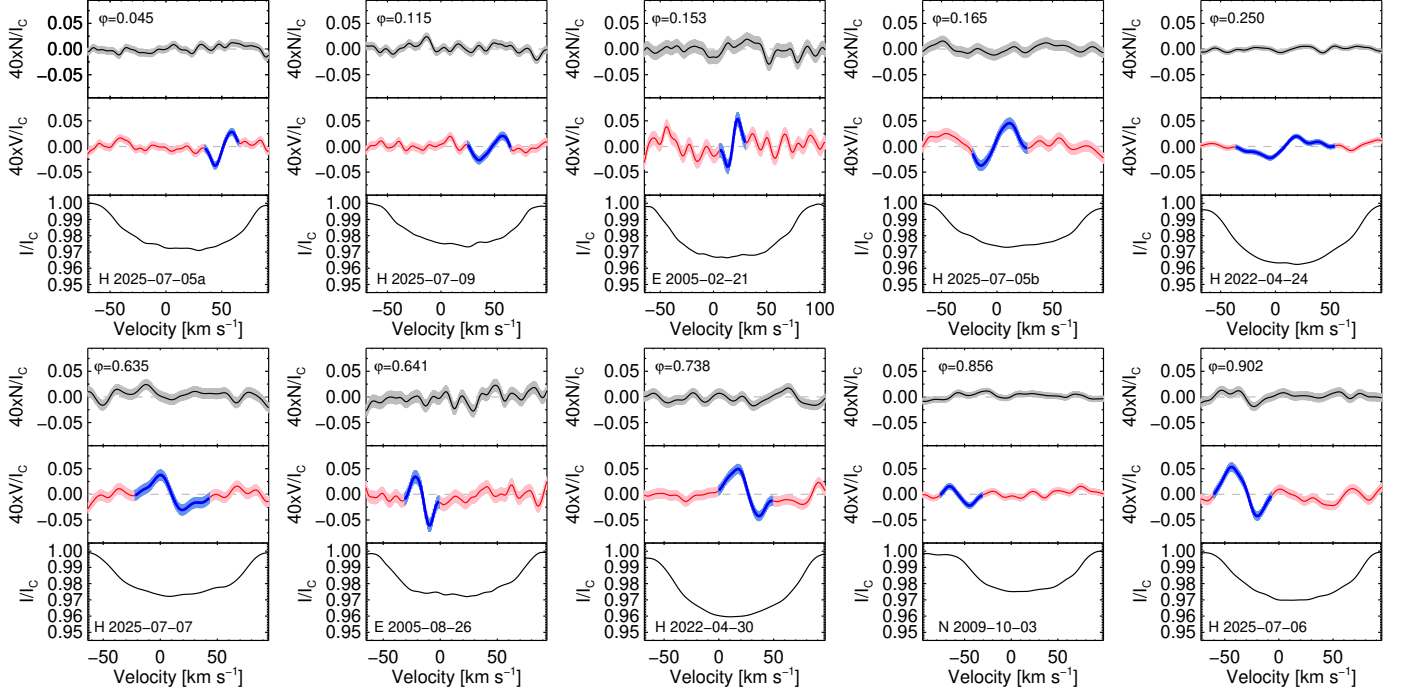


Fig. B.1. Least-squares deconvolution profiles. LSD Stokes I (bottom), Stokes V (middle), and diagnostic null (top) profiles for all epochs according to increasing phase. The Zeeman features are highlighted in blue.

Appendix C: LSD Stokes I profile variability observed for different elements

We show in Fig. C.1 the variable LSD Stokes I profiles calculated using Ti, Cr, and Fe lines.

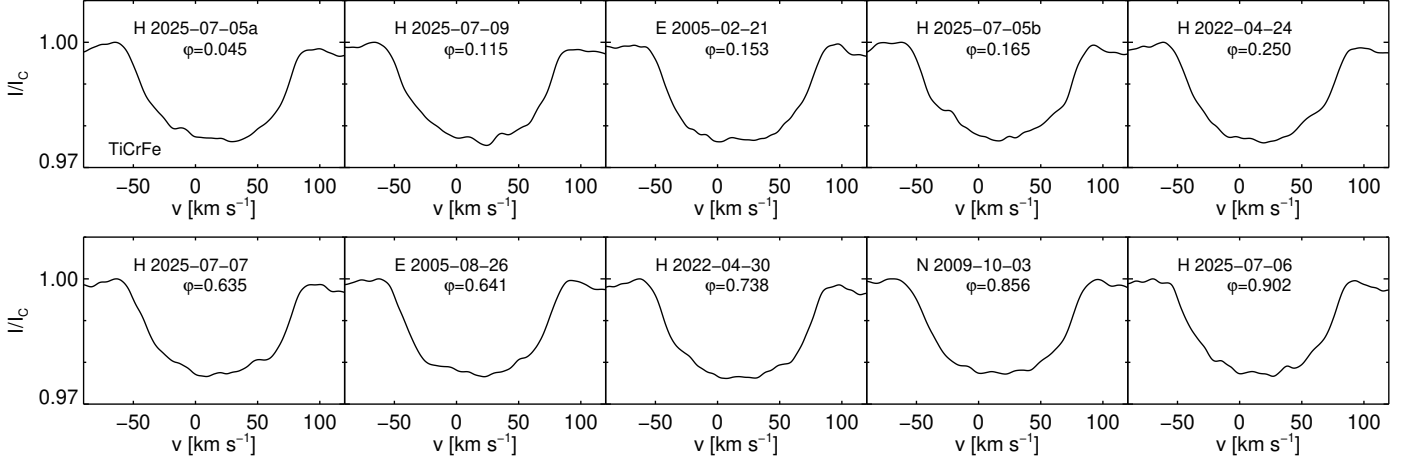


Fig. C.1. Least-squares deconvolution Stokes I profiles calculated using Ti, Cr, and Fe lines.

Appendix D: Line variability and additional periods

The $H\alpha$ profiles obtained in 2015 at $R = 14\,000$ have been intensively analysed by [Ismailov et al. \(2019\)](#). Neither $H\alpha$ nor $H\beta$ (dynamical spectrum and profiles visualised in Fig. D.1) show significant structure. This might be caused by some kind of dynamical process due to the presence of a companion. [Ismailov et al. \(2025\)](#) also suggested a longer period of $P_{\text{rot}} = 37.5$ d based on the analysis of $H\beta$ line variability. The dynamical spectrum using this period is presented in Fig. D.2. Albeit the phase coverage is poor, some hints of a structure with a maximum emission in phases between 0.15 and 0.4 are detected.

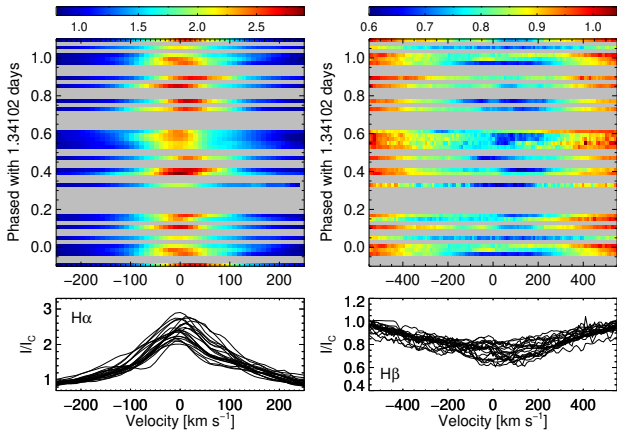


Fig. D.1. Same as Fig. 2 but showing only $H\alpha$ and $H\beta$ based on the 2015 lower resolution spectra.

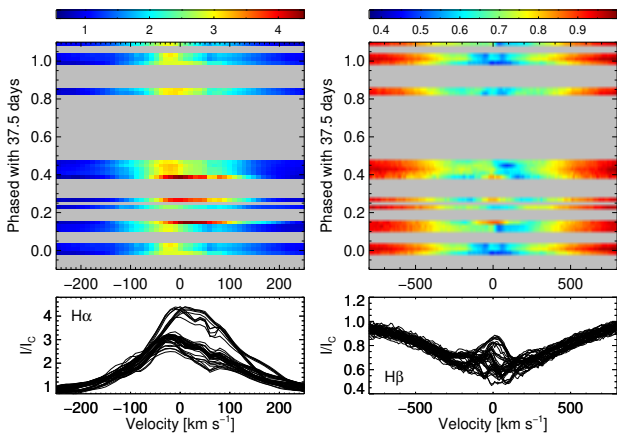


Fig. D.2. Same as Fig. 2 but phased with $P_{\text{rot}} = 37.5$ d, as suggested by [Ismailov et al. \(2025\)](#) and based on $H\beta$ variability.